



Copper porphyrin metal-organic framework modified carbon paper for electrochemical sensing of glyphosate

Rui Jiang^{a,c}, Yue-Hong Pang^{a,b}, Qiu-Yu Yang^{a,c}, Chao-Qun Wan^{a,c}, Xiao-Fang Shen^{a,b,c,d,*}

^a State Key Laboratory of Food Science and Technology, Jiangnan University, Wuxi 214122, China

^b International Joint Laboratory on Food Safety, Jiangnan University, Wuxi 214122, China

^c Institute of Analytical Food Safety, School of Food Science and Technology, Jiangnan University, Wuxi 214122, China

^d Key Laboratory of Synthetic and Biological Colloids, Ministry of Education, School of Chemical and Material Engineering, Jiangnan University, Wuxi 214122, China

ARTICLE INFO

Keywords:

Glyphosate
Copper porphyrin
Metal organic framework
Carbon paper
Electrochemical sensor

ABSTRACT

Glyphosate (GLY), an exceedingly effective herbicide, has raised worries about the risks posing to the ecosystem and human health due to excessive exposure. An electrochemical sensor based on copper porphyrin metal organic framework and gold nanoparticles modified carbon paper (Cu-TCPP/AuNPs/CP) was developed for sensitive determination of GLY by differential pulse voltammetry (DPV). The Cu-TCPP has large surface area and excellent catalytic activity, increasing the copper sites to combine with GLY for selective determination and improving the sensitivity of the electrochemical sensor. Under optimized conditions, the constructed sensor has a linear range from 0.2 to 120 $\mu\text{mol L}^{-1}$ with a detection limit of 0.03 $\mu\text{mol L}^{-1}$ (S/N = 3). The sensor was applied to water, soybean, wheat and carrot with the recovery ranging from 97.5% to 110.7%. After two weeks storage at 4 °C, the peak current of the sensor remains 86.6% of the original value with negligible interference. This sensor has a great potential application in water, soil and other environmental samples.

1. Introduction

Glyphosate (N-phosphonomethyl glycine, GLY), one of the most used non-selective organophosphorus herbicides, has widely applied to kill broadleaf plants and grasses in agricultural production and landscape maintenance [1]. The annual global production of GLY is about 825,800,000 kg, the increase of GLY usage is due to the release of GLY-resistant crops and the increase in “no-till” agriculture [2,3]. There is accumulating evidence that commercial herbicide formulations can result in increased oxidative stress and mitochondrial inhibition [4]. Consumers are indirectly exposed to GLY through food chain, such as water, fruits, beans and vegetables [5]. Bellé et al. [6] found that GLY and its metabolite change the cell cycle checkpoint by interfering with the physiological DNA repair mechanism. Cell cycle dysfunction can lead to chromosome instability and may increase the risk of cancer in humans. According to the Food and Agriculture Organization of the United Nations (FAO), the maximum residue limits (MRL) of GLY for meat, beans and milk are 0.05, 2 and 0.05 mg kg^{-1} , respectively. Consequently, it is necessary to develop a sensitive and convenient method for determination of GLY.

At present, the main detection methods for GLY include high-

performance liquid chromatography (HPLC) [7,8], spectrophotometry [9], electrophoresis [10], fluorescence [11] and electrochemiluminescence immunoassay [12]. Electrochemical sensor has the advantages of high sensitivity, fast analysis and economical application. However, GLY is electrically inactive [13,14] and difficult to be detected directly. Sheals et al. [15] found three donor groups of GLY (amine, carboxylate, phosphate) can form two five-membered equatorial planes with copper (II). Thereby, approaches based on indirect electrochemical sensor have been proposed using different working electrodes and modified materials. Setznagl et al. [16] detected GLY with a glassy carbon electrode modified with reduced graphene oxide and copper nanoparticles. Voltammetry tests show that the anodic peak decreases linearly with the addition of GLY at 30 mV due to the oxidation process of Cu^0 to Cu^{2+} . Regiart et al. [17] synthesized a nanoporous copper film with high porous and surface area, and successfully implemented for sensitive and selective detection of GLY. Thus, it is feasible to construct an electrochemical sensor based on the complex with copper ions for sensitive determination of GLY.

Conductive substrate of electrodes play an important role in electrochemical sensor. Traditional conductive substrate, such as glassy carbon electrode, is required to be polished and its electroactive area is

* Corresponding author at: State Key Laboratory of Food Science and Technology, Jiangnan University, Wuxi 214122, China.

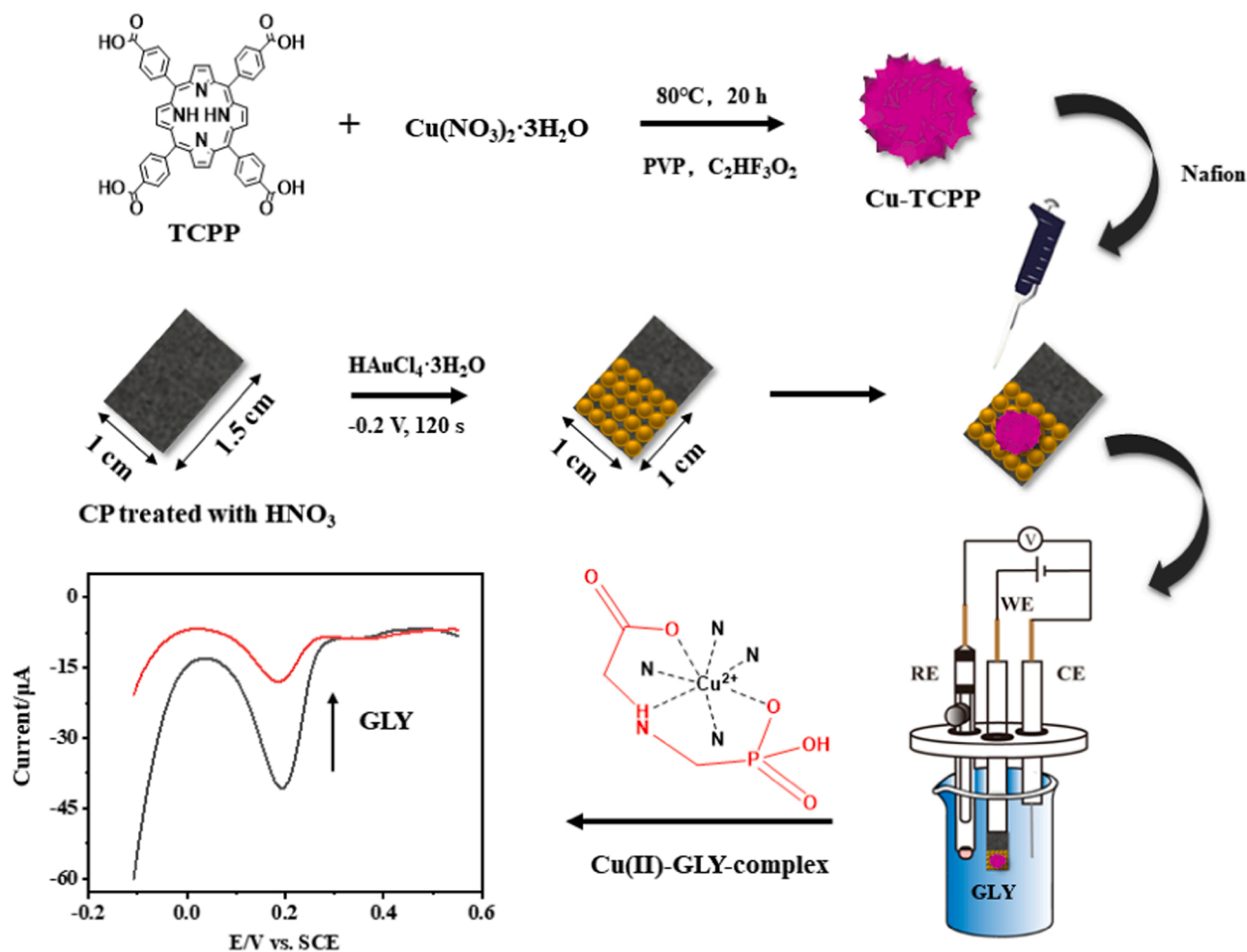
E-mail address: xfshen@jiangnan.edu.cn (X.-F. Shen).

<https://doi.org/10.1016/j.snb.2022.131492>

Received 17 November 2021; Received in revised form 23 January 2022; Accepted 24 January 2022

Available online 29 January 2022

0925-4005/© 2022 Elsevier B.V. All rights reserved.



Scheme 1. Scheme illustration of fabrication of the Cu-TCPP/AuNPs/CP electrode and electrochemical sensor for GLY.

small and limited [18]. Carbon paper (CP), composed of porous carbon fibers, presents with high conductivity, specific surface area and is suitable for mass production [19]. Compared with traditional electrodes, CP only needs to be cleaned without polishment and is less susceptible to oxidation. In recent years, CP has gradually applied for sensing consumed anti-inflammatory drugs, pesticides and nitrite [20–22].

In addition to conductive substrate of electrodes, the modification material on electrode is another important factor that affects the conductivity and sensitivity of the electrochemical sensor. Metal organic frameworks (MOFs) based sensors have emerged for detecting various targets, such as heavy metals, phenols and organophosphate pesticides. Among the various MOFs, porphyrin MOFs inherit porphyrin's unique large π conjugated structure and excellent optical and electrical properties. Porphyrin MOFs were used in electro-catalytic field because of its high catalytic activity with numerous exposed active sites on the surface and flexible structure [23–25]. Zhang et al. [26] used Cu-TCPP and poly(styrene sulfonate) functionalized graphene to construct a sensitive electrochemical sensor for simultaneous determination of dihydroxybenzene isomers. Liu et al. [27] chose silver nanoparticles functionalized 3D Cu-TCPP as a glassy electrode modifier, thus developing a novel electrochemical platform for the catalytic oxidation and quantitative detection of glutathione. These researches show that porphyrin MOFs are perspective candidates for electrochemical sensor.

In this work, the Cu-TCPP/AuNPs/CP sensor was fabricated by electrodeposition of AuNPs on CP and then coated with Cu-TCPP for detection of GLY. Two-dimensional layered structure of Cu-TCPP provided large specific surface area and copper sites, coordinating with GLY

selectively. Due to the synergistic electrocatalytic effect of Cu-TCPP and AuNPs, the constructed sensor show good conductivity and catalytic activity, successfully applied in water, soybean, carrot and wheat samples.

2. Experimental

2.1. Reagents and materials

The 2D MOFs Cu-TCPP was synthesized by solvothermal method [27]. GLY and (aminomethyl)phosphonic acid were purchased from Aladdin (Shanghai, China). Nafion was obtained from J&K Chemical (Beijing, China). Meso-tetra(4-carboxyphenyl)porphine (97%) (TCPP) was purchased from Enokay (Beijing, China). CP (thickness is 0.19 mm) was obtained from Hesen (Shanghai, China). Tetrachloroauric acid was purchased from Titan (Shanghai, China). 0.1 mol L⁻¹ acetic acid/sodium acetate (ABS) buffer solutions at pH 6 were prepared with sodium acetate anhydrous and glacial acetic, C₂H₄O₂ (99.4%). Metallic porphyrin MOFs were purchased from Aladdin (Shanghai, China). Organophosphorus pesticide was purchased from Macklin Biochemical Technology Co., Ltd. (Shanghai, China). HCl, CH₂Cl₂, Cu(NO₃)₂·3 H₂O, polyvinylpyrrolidone, trifluoroacetic acid, KCl, Fe(CN)₆³⁻, Fe(CN)₆⁴⁻, CuSO₄·5H₂O, MgSO₄, Na₂SO₄, CaCl₂·H₂O, CdCl₂·2.5H₂O, Pb(CH₃COO)₂·3H₂O, and FeSO₄·7H₂O were obtained from Sinopharm Chemical Reagent Co., Ltd. (Shanghai, China). A pattern solution 10 mmol L⁻¹ of GLY was prepared for experiment. All distilled water used in experiments was obtained from a Milli-Q system (Millipore, Bedford, USA).

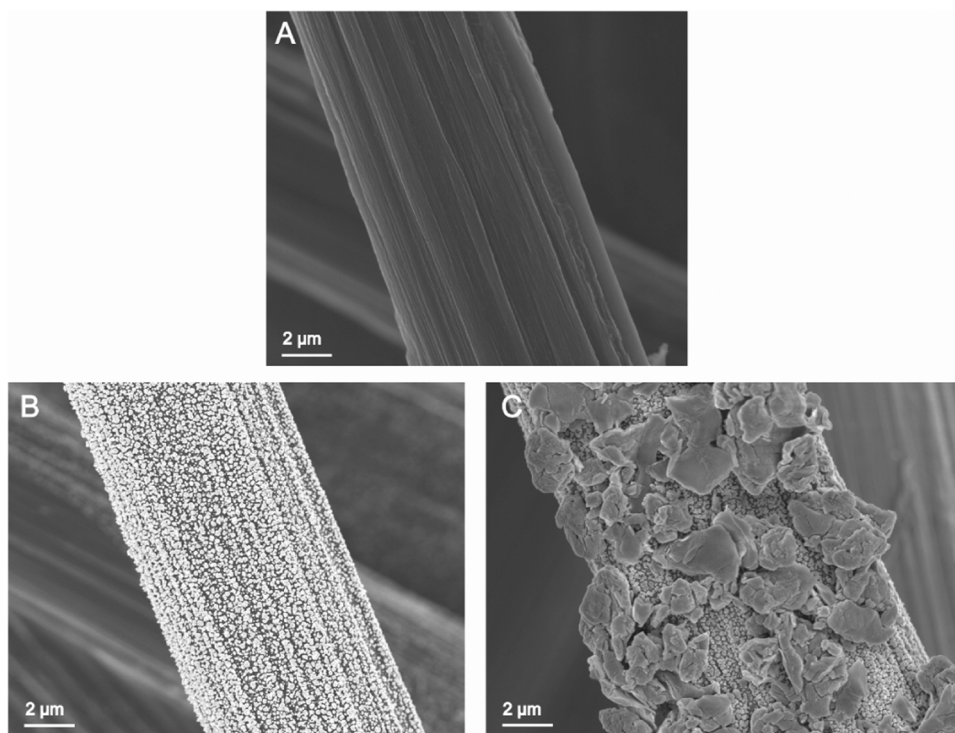


Fig. 1. SEM images of (A) CP treated with HNO_3 (B) AuNPs/CP and (C) Cu-TCPP/AuNPs/CP.

2.2. Apparatus

Saturated calomel electrode (SCE), CP working electrode (1 cm in width and 1.5 cm in total length) and Pt counter electrode consist of a three-electrode system. The electrochemical experiment was performed on a CHI 660c electrochemical workstation (Chenhua Instrument, Shanghai, China). The morphology of Cu-TCPP/AuNPs/CP was recorded on a SU8100 scanning electron microscope (SEM, Hitachi, Japan). N_2 adsorption experiment was performed on an Autosorb-iQ analyzer (Quantachrome, Boynton Beach, Florida, USA). The structural analysis of the Cu-TCPP was performed by a Fourier transform-infrared (FT-IR) spectrometer (Nicolet, USA). A dual beam UV-vis spectrophotometer (T9, Persee, Beijing, China) was used to characterize molecular structure of Cu-TCPP. The pH of the solutions was regulated by a pH meter (Mettler-Toledo, Switzerland). The solution was dispersed on a KQ-100DB CNC ultrasonic cleaner (Suzhou, China).

2.3. Fabrication of Cu-TCPP/AuNPs/CP electrodes

Before modification, the CP ($10 \times 15 \text{ mm}^2$) was ultrasonically cleaned in nitric acid: water (V:V=1:1), acetone and ethanol for 30 min. Then take out and vacuum dry at 60°C for use. The cleaned CP electrode was immersed in $\text{HAuCl}_4 \cdot 3\text{H}_2\text{O}$ (0.1%) solution, deposited at -0.2 V for 120 s [28] and dried at 60°C . Finally, the AuNPs/CP electrode was obtained. $30 \mu\text{L}$ Cu-TCPP nanomaterials were dispersed in water and 0.1% Nafion mixture (V:V=20:1), and dropped onto the surface of the AuNPs/CP electrode. Dry at 60°C and the Cu-TCPP/AuNPs/CP electrode was obtained for use.

2.4. Electrochemical measurement

The electrochemical characterization was performed via cyclic voltammetry (CV), differential pulse voltammetry (DPV) and electrochemical impedance spectroscopy (EIS). Cu-TCPP/AuNPs/CP was characterized by CV in a potential range from -0.2 – 0.6 V and EIS at an amplitude of 5 mV over a frequency range of 0.1 – 10^5 Hz in 1 mmol L^{-1}

$[\text{Fe}(\text{CN})_6]^{3-/4-}$ ($+0.2 \text{ mol L}^{-1} \text{ KCl}$). DPV measurements for GLY determination were recorded in a potential range from -0.2 – 0.6 V .

2.5. Samples preparation for GLY analysis

Soybean, wheat and carrot were purchased from the local supermarket and were treated according to the standard method (National Standards of the People's Republic of China GB/T 23750–2009). 10 mg of soybean flour, wheat flour and chopped carrots were taken in 50 mL distilled water with ultrasound treatment for 30 min. Then centrifugation was performed at 3500 r min^{-1} for 10 min and 20 mL supernatant was taken from the centrifuge tube. Then sonicate for 1 min and centrifuge for 5 min 15 mL supernatant and dichloromethane were added to centrifugal tube and centrifugation was performed for 5 min in order to remove fat. 4.5 mL supernatant was taken and 0.5 mL buffer was added. At last the mixture was filtered with $0.45 \mu\text{m}$ membrane and stored in the refrigerator at 4°C . In addition, $100 \mu\text{L}$ hydrochloric acid was added to soybean samples before removing the fat. Water obtained from the local supermarket was filtered with $0.45 \mu\text{m}$ membrane for analysis.

3. Results and discussion

3.1. Design of Cu-TCPP/AuNPs/CP sensor for GLY

The design of Cu-TCPP/AuNPs/CP electrochemical sensor for GLY is illustrated in Scheme 1. Firstly, Cu-TCPP was synthesized by solvothermal method [27]. Secondly, CP ($10 \times 10 \text{ mm}^2$) was treated with nitric acid and electro-deposited at -0.2 V for 120 s via immersing in 0.05% HAuCl_4 solution to improve conductivity of electrode (Fig. S1). The 0.7 mg mL^{-1} Cu-TCPP suspension ($30 \mu\text{L}$) was dropped onto the rectangular plane of CP. The addition of Nafion solution attached the Cu-TCPP to the electrode. Taking Cu-TCPP/AuNPs/CP as working electrode, saturated calomel electrode as reference electrode and Pt electrode as counter electrode, a three-electrode system was established. When GLY was added, it formed a complex structure with copper,

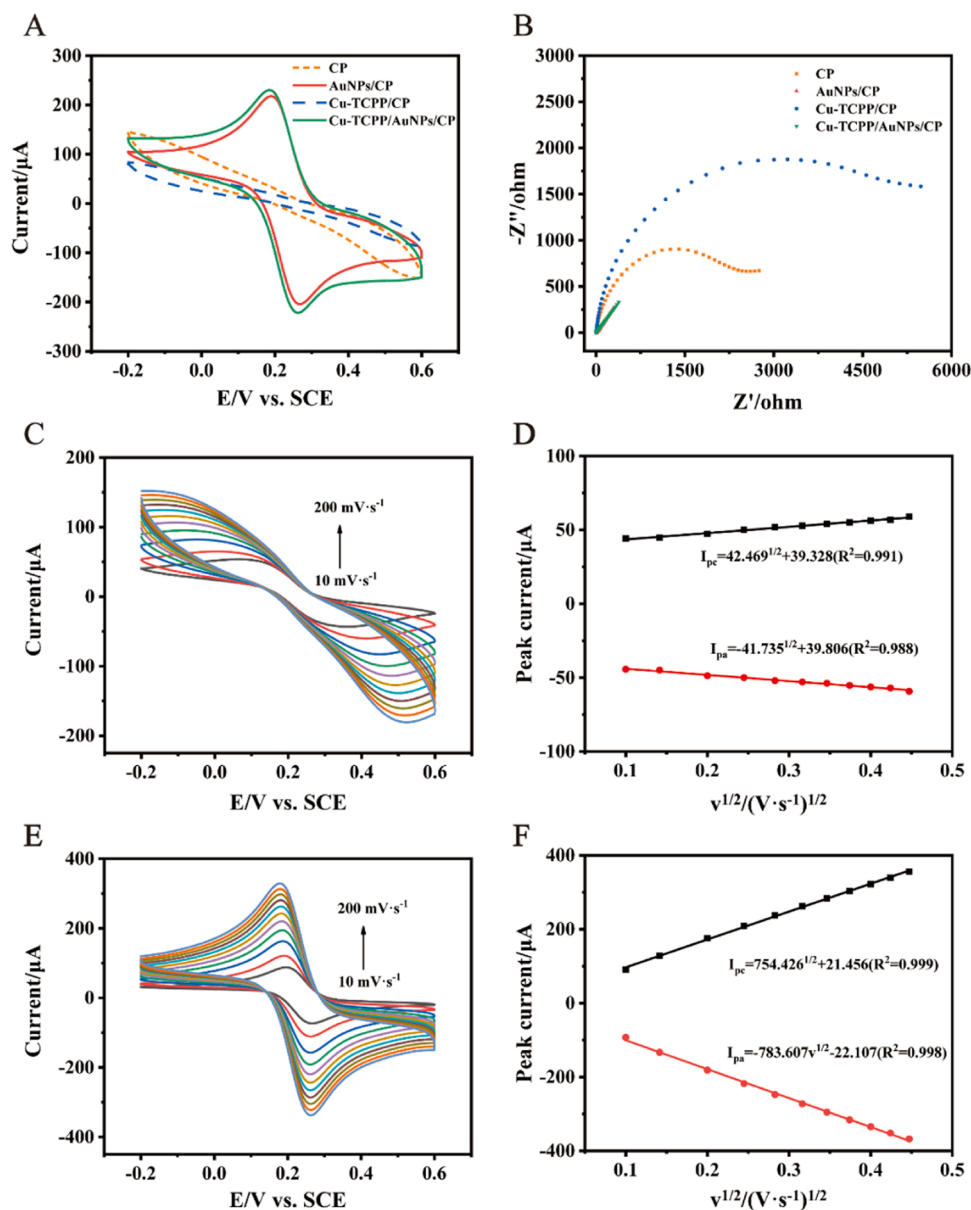


Fig. 2. (A) CV and (B) EIS of different modified electrodes in $1 \text{ mmol L}^{-1} [\text{Fe}(\text{CN})_6]^{3-}/[\text{Fe}(\text{CN})_6]^{4-}$ ($+0.2 \text{ mol L}^{-1} \text{ KCl}$). (C) CV curves of bare CP and (E) Cu-TCPP/AuNPs/CP at different scan rates of $10\text{--}200 \text{ mV s}^{-1}$. Linear relationship between peak currents of (D) bare CP or (F) Cu-TCPP/AuNPs/CP and scan rate $v^{1/2}$.

leading to the decrease oxidation peak current of copper. Finally, an electrochemical sensor based on Cu-TCPP/AuNPs/CP was established for determination of GLY.

3.2. Characterization of Cu-TCPP/AuNPs/CP electrode

The morphology of (A) CP treated with HNO_3 , AuNPs/CP and Cu-TCPP and Cu-TCPP/AuNPs were characterized by SEM. CP treated with HNO_3 (Fig. 1A) is composed of smooth carbon fiber in porous structure and the diameter of the carbon fiber is about $7 \mu\text{m}$. The nitrogen adsorption-desorption isotherm and the SEM image of CP show that it has porous structure (Fig. S2). The total pore volume of CP is $0.0627 \text{ cm}^3 \text{ g}^{-1}$, the calculated specific surface area of CP is $5.63 \text{ m}^2 \text{ g}^{-1}$. After electrodeposition, AuNPs are uniformly distributed on the surface of CP and its particle diameter is about 400 nm (Fig. 1B). Cu-TCPP are attached to the surface of AuNPs in sheet stacks (Fig. 1C). Moreover, the powder-like Cu-TCPP MOFs show a flower-like structure composed of ultrathin nanosheets. Its sheet stacks provide large specific surface area and an efficient π electron system on the electrode surface (Fig. S3).

While Cu-TCPP are dissolved in Nafion solution and treated ultrasonically, the flower like structure of Cu-TCPP MOFs are scattered.

In addition, the successful coordination of TCPP with Cu^{2+} was confirmed by FTIR. FT-IR spectra of TCPP and Cu-TCPP show characteristic absorption peaks of large ring skeletons at 716 cm^{-1} and 1000 cm^{-1} (Fig. S4). The peak at 1403 cm^{-1} corresponds to the tensile vibration of the C=N bond of the pyrrole ring. The absorption peaks of 1108 cm^{-1} and 1607 cm^{-1} are the skeleton vibration of the external benzene ring, the vibration peak of C=O on the carboxyl group is at 1660 cm^{-1} , and the characteristic peak of benzene ring substitution is at 772 cm^{-1} . Compared with TCPP, the peak strength at 1270 cm^{-1} of Cu-TCPP nanomaterials is significantly reduced because hydrogen on -OH is replaced by metal ions to form Cu-O bonds, indicating that Cu^{2+} is coordinated with the carboxyl group of TCPP. The characteristic peak at 1000 cm^{-1} is attributed to the stretching vibration absorption of N-Cu bond, indicating that the metal ion Cu^{2+} in the synthesized metal porphyrin derivatives has formed coordination compounds with the porphyrin ring [29]. UV-vis absorption spectra of Cu-TCPP is shown in Fig. S5. The characteristic absorption Soret band of TCPP is at 420 nm ,

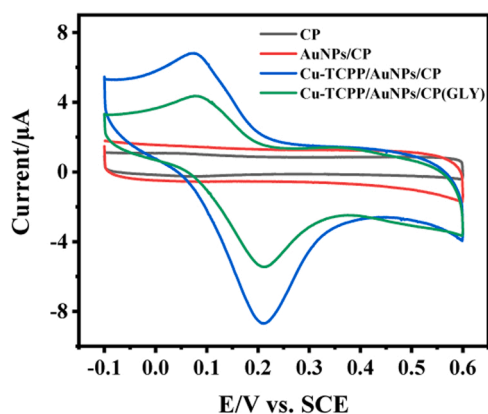


Fig. 3. CV scans in ABS (pH 6) at a scan rate of 50 mV s^{-1} of CP, AuNPs/CP, Cu-TCPP/AuNPs/CP, Cu-TCPP/AuNPs/CP (GLY) electrode.

which is mainly the result of the transition of electrons from three inner occupied orbitals of porphyrins to lower energy orbitals. UV-vis absorption spectrum of Cu-TCPP is at 548 nm and shows Q band absorption induced by metal coordination. The presence of cationic bands at 420 nm and accompanying shoulder bands at 438 nm may result from the aggregation of MOF nanosheets.

3.3. The electrochemical characterization of Cu-TCPP/AuNPs/CP

CV was used to investigate the electrochemical characterization of different electrodes in a $1 \text{ mmol L}^{-1} [\text{Fe}(\text{CN})_6]^{3-}/[\text{Fe}(\text{CN})_6]^{4-}$ solution (containing $0.2 \text{ mol L}^{-1} \text{ KCl}$) at a scanning rate of 100 mV s^{-1} . Peak current of glassy carbon electrode, indium tin oxide, pencil graphite

electrode and CP is $14.2 \mu\text{A}$, $75.8 \mu\text{A}$, $43.7 \mu\text{A}$ and $182.2 \mu\text{A}$ (Fig. S6). Compared with the conventional electrodes, CP has better conductivity due to its large specific surface area. The bare CP electrode shows reversible redox peak currents of $-145.7 \mu\text{A}$ and $144.3 \mu\text{A}$. The Cu-TCPP/AuNPs/CP electrode shows a pair of reversible redox peaks with potential difference of 77 mV and peak current of $-223.5 \mu\text{A}$ and $206.5 \mu\text{A}$, respectively (Fig. 2A). The redox peak currents of the Cu-TCPP/AuNPs/CP electrode are higher than those of the bare CP electrode, indicating that Cu-TCPP/AuNPs/CP electrode has better conductivity. Compared with the AuNPs/CP electrode, the conductivity of Cu-TCPP/AuNPs/CP is slightly improved. This phenomenon is not only a simple addition of AuNPs and Cu-TCPP, but mainly the synergistic effect between AuNPs and Cu-TCPP, which improves the electrode surface performance and accelerates the electron transfer rate.

The charge transfer property of different electrodes was investigated by EIS. As is shown in Fig. 2B, the charge transfer resistance (R_{ct}) of Cu-TCPP/CP (7000Ω) has the highest impedance, which is attributed to the weak conductivity of two-dimensional MOFs. Two-dimensional MOF materials have a high stacking tendency, leading to a reduction of exposed active sites and a limitation of electron transfer. However, the R_{ct} of the Cu-TCPP/AuNPs/CP electrode (25Ω) decreases significantly because AuNPs increases the electroactive area of CP and improves the conductivity of the electrode.

CV method was used to investigate the electrochemical active area of the modified electrode in the redox probe at different scan rates (Fig. 2). In the range of $10\text{--}200 \text{ mV s}^{-1}$, the redox peak currents of the modified electrode increases linearly with the increase of the scan rate. The linear equation of redox peak currents and $v^{1/2}$ of CP electrode are $I_{pa} (\mu\text{A}) = 41.735v^{1/2} + 39.806$ ($R^2 = 0.998$) and $I_{pc} (\mu\text{A}) = 42.469v^{1/2} + 39.328$ ($R^2 = 0.991$) (Fig. 2C, 2D). The linear equation of redox peak currents and $v^{1/2}$ of Cu-TCPP/AuNPs/CP electrode are $I_{pa} (\mu\text{A}) = 783.607v^{1/2}$.

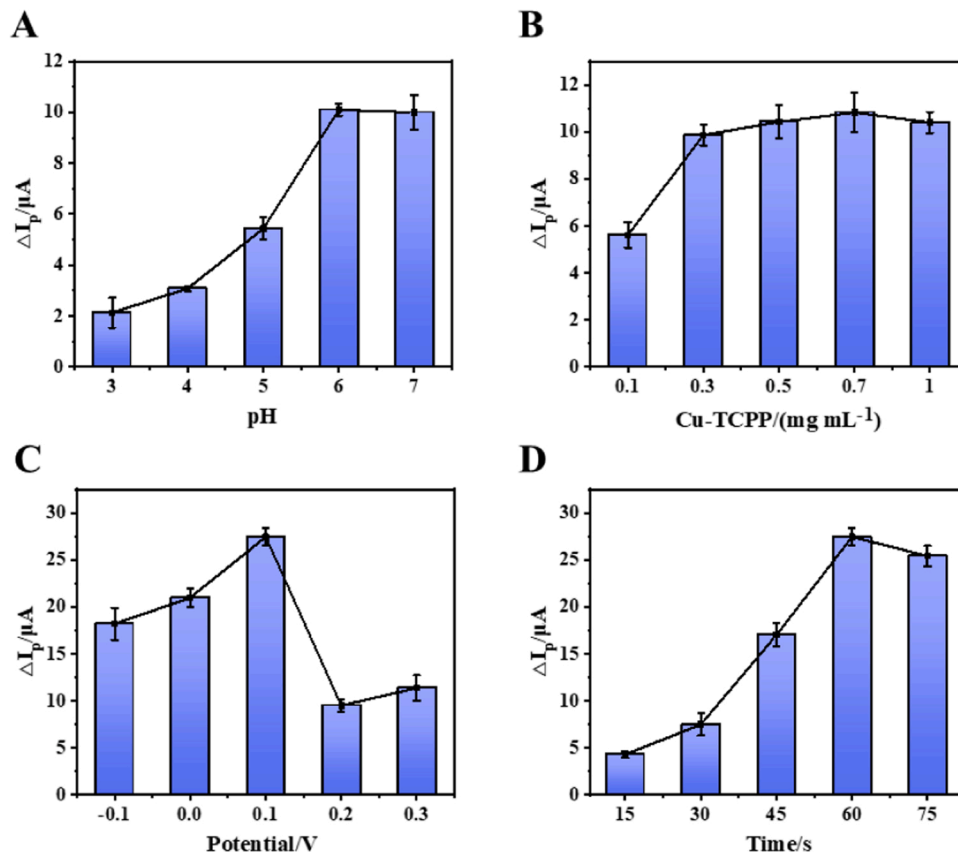


Fig. 4. Optimization of (A) pH values (B) concentration of Cu-TCPP (C) enrichment potential and (D) enrichment time (ΔI_p represents the difference between the peak current of Cu-TCPP/AuNPs/CP in the absence and presence of GLY).

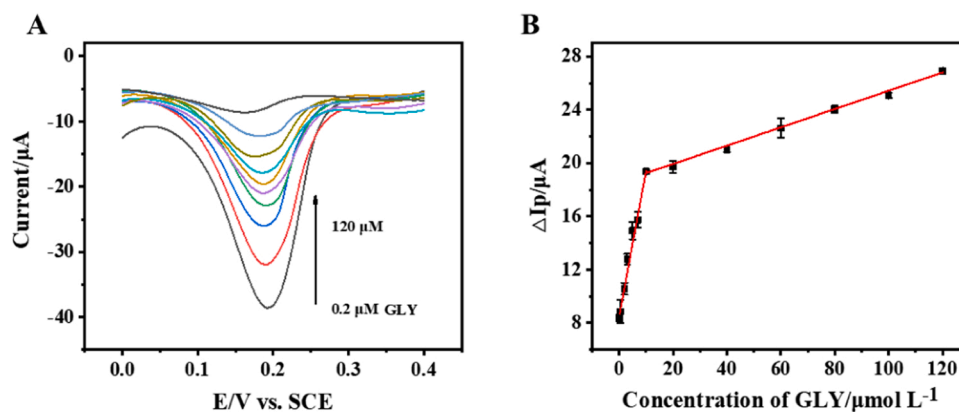


Fig. 5. . (A) DPV of the sensor to GLY (B) The relationship between oxidation peak current of GLY and its concentration.

22.107 ($R^2 = 0.998$) and $I_{pc} (\mu A) = 754.426v^{1/2} + 21.456$ ($R^2 = 0.999$) (Fig. 2E, 2F). According to Randles-Sevcik equation [30], the electroactive area of Cu-TCPP /AuNPs/CP was calculated as follows:

$$I_p = 268600n^{3/2}AD^{1/2}Cv^{1/2}$$

I_p is the anodic peak current (μA), n is the electron transfer number of the redox reaction ($n = 1$), A is the electrochemical active area of the modified electrode, D is the diffusion coefficient of ferricyanide ($D = 7.60 \times 10^{-6} \text{ cm}^2 \text{ s}^{-1}$), C is the concentration of $[\text{Fe}(\text{CN})_6]^{3-/4-}$ (mol cm^{-3}) and v is the scan rate (V s^{-1}). We found that the electroactive area of the Cu-TCPP and AuNPs modified electrode increases significantly, which is 18.8 times larger than that of the bare CP electrode.

3.4. The electrochemical behavior of GLY

To investigate the electrochemical behavior of the electrode in GLY solution, CV curves for three different modified electrodes were compared (Fig. 3). There is no reversible redox peaks at the bare CP and AuNPs/CP electrode, because the target GLY rarely shows the electrochemical activity at an accessible potential. However, an obvious anodic peak was generated at 0.192 V by Cu-TCPP/AuNPs/CP, indicating the oxidation of copper. When $20 \mu\text{mol L}^{-1}$ GLY was added in ABS buffer, the peak anodic current of Cu^{2+} decreased. The inhibition of GLY adsorption to Cu-TCPP explained the variation of the current peak. Compared with other common pesticides, GLY contains both P=O, C=O and N-H chelating groups, which has a strong affinity with Cu^{2+} . This inhibition is contrary to what has been reported in other pesticide detection studies. It maybe because GLY forms a complex with the Cu^{2+} of Cu-TCPP, which reduces the exposure of Cu-TCPP on the electrode surface and thus inhibits the peak current. Coutinho et al. [31] found that the strong interaction between GLY and Cu^{2+} ions forms a stable complex that allows indirect electrochemical detection of GLY. Moreover, CV method was adopted to investigate the effects of different

Table 1
Studies reporting GLY quantification using electrochemical methods.

Electrodes/methods	Linear range ($\mu\text{mol L}^{-1}$)	LOD ($\mu\text{mol L}^{-1}$)	Ref.
Cu^{2+} -Cu/GC/DPV	4–30	0.19	(Aguirre et al.) [32]
Electrogenerated NiAl-LDH/films/ampereometric	10–300	5	(Khenifi et al.) [33]
GC/MWCNT/CuPc/DPV	830–9900	11.9	(Noori et al.) [34]
SPE/Au/Amperometric	300–2000	1.6	(Moraes et al.) [35]
GrO-PE/SWV	18–1200	0.017	(Jaqueline et al.) [36]
Cu-TCPP/AuNPs/CP/DPV	0.2–120	0.03	This work

porphyrin MOFs on GLY (Fig. S7). Iron porphyrin MOFs and zinc porphyrin MOFs have no obvious effects on GLY, while Cu-TCPP coordinates with GLY and the oxidation peak current has a significant decrease. Cu-TCPP can combine with GLY selectively among the other porphyrin MOFs.

3.5. Optimization of parameters for GLY analysis

In order to obtain high sensitivity of electrochemical sensor, some important experimental parameters were optimized, including pH, Cu-TCPP concentration, enrichment potential and enrichment time. ΔI_p represents the difference between the peak current of Cu-TCPP/AuNPs/CP in the absence and presence of GLY.

The influence of pH on the peak current of Cu-TCPP/AuNPs/CP in the absence and presence of GLY was investigated by DPV (Fig. 4A). The results show that ΔI_p increases gradually with the increase of pH value, indicating that the proton participates in the reaction process between Cu-TCPP/AuNPs/CP and GLY. ΔI_p of Cu-TCPP/AuNPs/CP tends to be stable at higher pH values. Considering the effect of pH on the oxidation current of Cu^{2+} , ABS buffer with pH 6 was selected for detection of GLY.

On the other hand, the amount of Cu-TCPP on the electrode surface has influence on the sensitivity of the sensor. DPV method was employed to investigate the influence of Cu-TCPP on the electrode surface. ΔI_p has reached the maximum with 0.7 mg mL^{-1} Cu-TCPP (Fig. 4B). ΔI_p decreases with the amount of Cu-TCPP increasing gradually, which may result from the agglomeration of materials. Thus, 0.7 mg mL^{-1} was selected as the optimal concentration on the surface of the Cu-TCPP/AuNPs/CP electrode.

In order to obtain the better sensitivity, we also optimized the potential enrichment of GLY on the surface of Cu-TCPP/AuNPs/CP electrode (Fig. 4C). Under acidic conditions, GLY is negatively charged. Positive voltage can drive GLY to accumulate on the electrode surface, so ΔI_p increases at -0.1 – 0.1 V. The oxidation potential of Cu^{2+} is near 0.192 V, when the copper is completely oxidized at 0.1 V, the surface of the electrode copper ion saturates and partial dissolves at the electrode surface, ΔI_p decreases at 0.1–0.3 V. Therefore, we chose 0.1 V as the optimal enrichment potential.

The effect of deposition time of GLY on the surface of Cu-TCPP/AuNPs/CP electrode was investigated in 0.1 mol L^{-1} ABS buffer solution (pH = 6). Because of the enrichment of GLY on the electrode surface, ΔI_p increases with the increasing of deposition time (Fig. 4D). After 60 s, ΔI_p tends to decrease due to the saturation of GLY at the electrode. At last, 60 s was selected as the optimal deposition time.

3.6. Analytical curve, the limit of detection and quantification

Determination of GLY at different concentrations was investigated by DPV under optimized conditions (Fig. 5). In the concentration range of

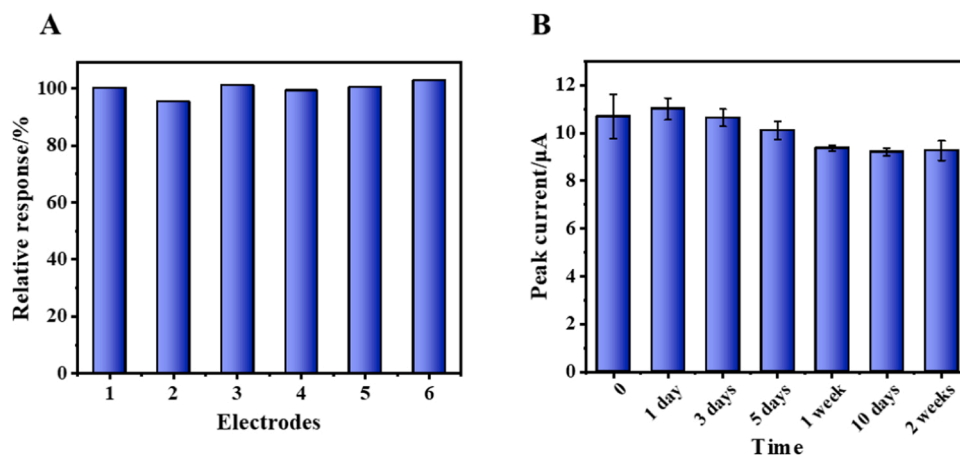


Fig. 6. (A) Relative response measured with six different modified electrodes in 0.1 mol L^{-1} ABS (pH 6.0) with $10 \mu\text{mol L}^{-1}$ (B) Peak current measured with different storage days of Cu-TCP/AuNPs/CP electrode. Points and bars are means and standard deviations of three electrodes.

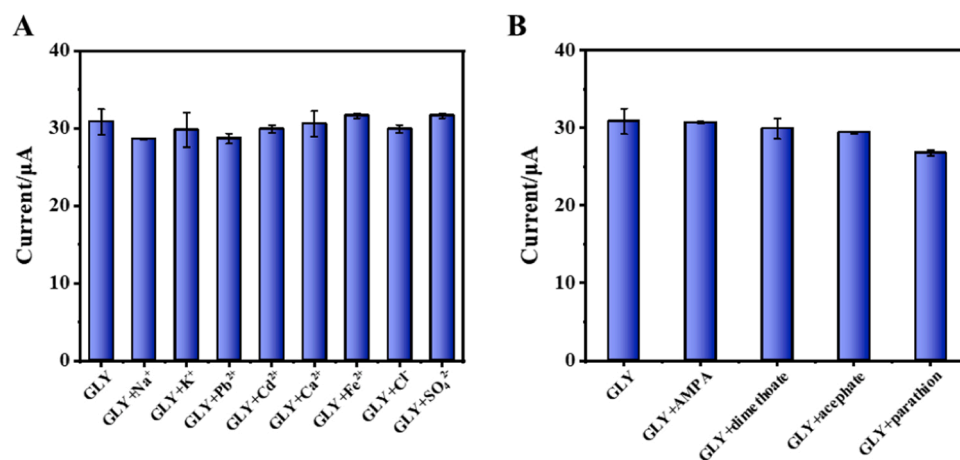


Fig. 7. Peak current values measured with Cu-TCP/AuNPs/CP electrode containing $2 \mu\text{mol L}^{-1}$ GLY in the absence and presence of (A) anions and cations ($200 \mu\text{mol L}^{-1}$) and (B) $2 \mu\text{mol L}^{-1}$ organophosphorus pesticides.

$0.2\text{--}120 \mu\text{mol L}^{-1}$, the oxidation peak current decreases with the increase of GLY concentration with two linear relationships. The regression equation is $\Delta I_p (\mu\text{A}) = 1.0932 C_{\text{GLY}} + 8.4697$ ($R^2 = 0.994$) at low concentrations ($0.02\text{--}10 \mu\text{mol L}^{-1}$) and $\Delta I_p (\mu\text{A}) = 0.0687 C_{\text{GLY}} + 18.562$ ($R^2 = 0.996$) at high concentrations ($10\text{--}120 \mu\text{mol L}^{-1}$). The detection limit of GLY is $0.03 \mu\text{mol L}^{-1}$ ($S/N = 3$), which can be used to monitor the concentration of GLY in real samples under the current regulatory limit.

Compared with the performance of the electrochemical sensor previously reported for the detection of GLY, the sensor established in this paper has a wider linear range with a lower detection limit (Table 1). The disposable electrodes are cheap and convenient with simple pretreatment. Cu-TCP/AuNPs/CP provides a considerable platform for electrochemical sensing of GLY.

3.7. Reproducibility, stability and selectivity of the Cu-TCP/AuNPs/CP

The reproducibility, interference and stability of the electrode were investigated under the optimized conditions. To study the reproducibility of the sensor, six Cu-TCP/AuNPs/CP electrodes were prepared using the same modification method and the same concentration of GLY solution was detected. As is shown in the Fig. 6A, the relative standard deviation was calculated to be 2.5%, indicating that the sensor has good reproducibility. After two weeks storage at 4°C , the peak current of the sensor remains 86.6% of the original value (Fig. 6B). It is indicated that

Table 2

Determination of GLY in food samples ($n = 3$).

Samples	Added ($\mu\text{mol L}^{-1}$)	Found ($\mu\text{mol L}^{-1}$)	Recovery (%)	RSD (%)
Soybean	0	6.35	–	3.8
	1	8.96	110.7	8.0
	5	9.87	99.5	3.5
	10	14.33	99.3	4.1
Carrot	0	ND	–	–
	1	0.82	97.9	4.9
	5	4.97	99.8	1.8
	10	9.89	99.4	2.8
Wheat	0	ND	–	–
	1	0.93	99.2	3.9
	5	5.44	103.5	4.1
	10	9.63	97.9	1.0
Water	0	ND	–	–
	1	0.93	97.5	8.8
	5	5.03	102.8	7.0
	10	10.69	100.2	0.8

the fabricated sensor has acceptable stability and reproducibility for the detection of GLY.

In addition, the anti-interference of the sensor was evaluated by adding cation and anion with 100-fold concentration higher than that of $2 \mu\text{mol L}^{-1}$ GLY and $2 \mu\text{mol L}^{-1}$ organophosphorus pesticides. In this study, two kinds of interfering substance were analyzed, one group using

the main metabolite AMPA of GLY and organophosphorus pesticides. The other group includes common anions and cations in the sample (Na^+ , K^+ , Pb^{2+} , Cd^{2+} , Ca^{2+} , Fe^{2+} , Cl^- , SO_4^{2-}), which may interfere with measurement. The experimental results shows that these interference substances do not interfere with the electrochemical sensing of GLY. (Fig. 7).

3.8. Determination of GLY in food samples

The practical application of Cu-TCPP/AuNPs/CP was verified by the determination of GLY in soybean, carrot, wheat and water samples in Table 2. GLY was found in soybean with levels of $6.35 \mu\text{mol L}^{-1}$, meeting the requirements of the Codex Alimentarius Commission (CAC) standard limits. Standard addition method was used for recovery test, and the accuracy of the sensor was evaluated. The recovery of GLY range from 97.5% ~ 110.7% (RSDs <10.0%) in these four food samples.

4. Conclusion

We reported the fabrication of a convenient and sensitive electrochemical sensor based on CP modified with Cu-TCPP and AuNPs for determination of GLY. CP was used as the novel working electrode for determination of GLY for the first time and Cu-TCPP with large surface area and excellent catalytic activity was helpful to improve electrochemical sensing performance. The developed sensor has a low detection limit, good reproducibility and anti-interference ability. Moreover, the disposable CP electrode is convenient for mass production and on-site rapid detection, which provides an effective analysis tool for on-site environmental monitoring and food safety control.

CRedit authorship contribution statement

Rui Jiang: Conceptualization, Methodology, Formal analysis, Investigation, Writing – Original Draft. **Xiao-Fang Shen:** Conceptualization, Resources, Writing – review & editing, Project administration, Funding acquisition. **Yue-Hong Pang:** Methodology, Formal analysis, Validation, Funding acquisition. **Qiu-Yu Yang:** Conceptualization, Methodology. **Chao-Qun Wan:** Investigation, Data Curation.

Declaration of Competing Interest

The authors report no declarations of interest.

Acknowledgments

This work was supported by the National Natural Science Foundation of China (22076067, 21976070) and the Fundamental Research Funds for the Central Universities (JUSRP22003).

Appendix A. Supporting information

Supplementary data associated with this article can be found in the online version at [doi:10.1016/j.snb.2022.131492](https://doi.org/10.1016/j.snb.2022.131492).

References

- A.D. Baylis, Why glyphosate is a global herbicide: strengths, weaknesses and prospects, *Pest Manag. Sci.* 56 (2000) 299–308, [https://doi.org/10.1002/\(sici\)1526-4998\(200004\)56:4<299::Aid-ps144>3.0.Co;2-k](https://doi.org/10.1002/(sici)1526-4998(200004)56:4<299::Aid-ps144>3.0.Co;2-k).
- C.M. Benbrook, Trends in glyphosate herbicide use in the United States and globally, *Environ. Sci. Eur.* 28 (2016) 3, <https://doi.org/10.1186/s12302-016-0070-0>.
- J. Xu, S. Smith, G. Smith, W. Wang, Y. Li, Glyphosate contamination in grains and foods: an overview, *Food Control* 106 (2019), <https://doi.org/10.1016/j.foodcont.2019.106710>.
- D.C. Bailey, C.E. Todt, S.L. Burchfield, A.S. Pressley, R.D. Denney, I.B. Snapp, R. Negga, W.L. Traynor, V.A. Fitsanakis, Chronic exposure to a glyphosate-containing pesticide leads to mitochondrial dysfunction and increased reactive oxygen species production in *Caenorhabditis elegans*, *Environ. Toxicol. Pharmacol.* 57 (2018) 46–52, <https://doi.org/10.1016/j.etap.2017.11.005>.
- L.P. Agostini, R.S. Dettogni, R. Reis, E. Stur, I.D. Louro, Effects of glyphosate exposure on human health: insights from epidemiological and in vitro studies, *Sci. Total Environ.* 705 (2019), 135808, <https://doi.org/10.1016/j.scitotenv.2019.135808>.
- R. Bellé, R. Le Bouffant, J. Morales, B. Cosson, P. Cormier, O. Mulner-Lorillon, Sea urchin embryo, DNA-damaged cell cycle checkpoint and the mechanisms initiating cancer development, *J. De. la Société De. Biol.* 201 (2007) 317–327, <https://doi.org/10.1051/jbio:2007030>.
- R. Exterkoetter, D.E. Rozane, W.C. da Silva, A.T. Toci, G.A. Cordeiro, S.F. Benassi, M. Boroski, Potential of terracing to reduce glyphosate and AMPA surface runoff on Latosol, *J. Soils Sediment.* 19 (2019) 2240–2250, <https://doi.org/10.1007/s11368-018-2210-1>.
- M. Ofitserova, S.J. Nerkar, Glyphosate analysis in foods by HPLC with postcolumn derivatization and fluorescence detection, *LC-GC North Am.* 35 (2017), S18–S18, (<https://link.gale.com/apps/doc/A600696626/AONE?u=anon~ed6e5e3d&sid=googleScholar&xid=bc7d9f08>).
- A. Romero-Natale, I. Palchetti, M. Avelar, E. Gonzalez-Vergara, J. Luis Garate-Morales, E. Torres, Spectrophotometric Detect. glyphosate Water Complex Form. bis 5-phenyldipyrinate Nickel (II) glyphosate, *Water* 11 (2019), <https://doi.org/10.3390/w11040719>.
- J. Liu, W. Feng, M. Tian, L. Hu, Q. Qu, L. Yang, Titanium dioxide-coated core-shell silica microspheres-based solid-phase extraction combined with sheathless capillary electrophoresis-mass spectrometry for analysis of glyphosate, glufosinate and their metabolites in baby foods, *J. Chromatogr. A* (2021) (1659), <https://doi.org/10.1016/j.chroma.2021.462519>.
- L. Bouzada, S. Hernandez, S. Kergaravat, Glyphosate detection from commercial formulations: comparison of screening analytic methods based on enzymatic inhibition, *Int. J. Environ. Anal. Chem.* (2019) 1–15, <https://doi.org/10.1080/03067319.2019.1691176>.
- H. Liu, P. Chen, Z. Liu, J. Liu, J. Yi, F. Xia, C. Zhou, Electrochemical luminescence sensor based on double suppression for highly sensitive detection of glyphosate, *Sens. Actuators B Chem.* 304 (2020), <https://doi.org/10.1016/j.snb.2019.127364>.
- R. Bataller, I. Campos, N. Laguarda-Miro, M. Alcañiz, J. Soto, R. Martínez-Mañez, L. Gil, E. García-Breijo, J. Ibáñez-Civera, Glyphosate detection by means of a voltammetric electronic tongue and discrimination of potential interferents, *Sensors* 12 (2012) 528–536, <https://doi.org/10.3390/s121217553>.
- L.A. Zambrano-Intriago, C.G. Amorim, J.M. Rodriguez-Diaz, A.N. Araujo, M. Montenegro, Challenges in the design of electrochemical sensor for glyphosate-based on new materials and biological recognition, *Sci. Total Environ.* 793 (2021) 17, <https://doi.org/10.1016/j.scitotenv.2021.148496>.
- J. Sheals, P. Persson, B. Hedman, IR and EXAFS spectroscopic studies of glyphosate protonated and copper(II) complexes of glyphosate in aqueous solution, *Inorg. Chem.* 40 (2001) 4302, <https://doi.org/10.1021/ic000849g>.
- S. Setznagl, I. Cesarino, Copper nanoparticles and reduced graphene oxide modified a glassy carbon electrode for the determination of glyphosate in water samples, *Int. J. Environ. Anal. Chem.* (2020) 1–13, <https://doi.org/10.1080/03067319.2020.1720667>.
- M. Regiart, A. Kumar, J.M. Goncalves, G.J. Silva Junior, J.C. Masini, L. Angnes, M. Bertotti, An electrochemically synthesized nanoporous copper microsensor for highly sensitive and selective determination of glyphosate, *Chemelectrochem* 7 (2020) 1558–1566, <https://doi.org/10.1002/celec.202000064>.
- M. Chandramouli, V.K. Boraiah, R.P. Shivalingappa, V. Basavanna, S. Doddamani, S. Ningaiah, Paper-based carbon dioxide sensors: past, present, and future perspectives, *Biointerface Res. Appl. Chem.* 12 (2022) 2353–2360, <https://doi.org/10.33263/briac122.23532360>.
- J. Zhao, D. Huo, X. Geng, J. Bao, J. Hou, Z. Shui, H. Yang, Y. Qi, Y. Hu, M. Yang, C. Hou, 3D MoS₂-AuNPs carbon paper probe for ultrasensitive detection and discrimination of p53 gene, *Sens. Actuators B Chem.* 332 (2021), <https://doi.org/10.1016/j.snb.2021.129480>.
- A. Torrinha, M. Martins, M. Tavares, C. Delerue-Matos, S. Morais, Carbon paper as a promising sensing material: characterization and electroanalysis of ketoprofen in wastewater and fish, *Talanta* 226 (2021), 122111, <https://doi.org/10.1016/j.talanta.2021.122111>.
- T. Wang, R.C. Reid, S.D. Minter, A paper-based mitochondrial electrochemical biosensor for pesticide detection, *Electroanalysis* 28 (2016) 854–859, <https://doi.org/10.1002/elan.201500487>.
- Y. Wan, Y.F. Zheng, H.Y. Yin, X.C. Song, Au nanoparticle modified carbon paper electrode for an electrocatalytic oxidation nitrite sensor, *New J. Chem.* 40 (2016) 3635–3641, <https://doi.org/10.1039/c5nj02941d>.
- S. Zhu, X. Lin, P. Ran, Q. Xia, C. Yang, J. Ma, Y.J. Fu, A novel luminescence-functionalized metal-organic framework nanoflowers electrochemiluminescence sensor via “on-off” system, *Biosens. Bioelectron.* 91 (2017) 436–440, <https://doi.org/10.1016/j.bios.2016.12.069>.
- B. Han, X. Ou, Z. Deng, Y. Song, C. Tian, H. Deng, Y.J. Xu, Z.J. Lin, Nickel metal-organic framework monolayers for photoreduction of diluted CO₂: metal-node-dependent activity and selectivity, *Angew. Chem. Int. Ed.* 57 (2018) 16811–16815, <https://doi.org/10.1002/anie.201811545>.
- J.H. Liu, L.M. Yang, E.J. Ganz, Electrochemical reduction of CO₂ by single atom catalyst TM-TCNQ monolayers, *J. Mater. Chem. A* 7 (2019) 3805–3814, <https://doi.org/10.1039/C8TA08677J>.
- C.J. Zhang, M.M. Han, L.L. Yu, L.B. Qu, Z.H. Li, Fabrication an electrochemical sensor based on composite of Cu-TCPP nanosheets and PSS functionalized graphene for simultaneous and sensitive determination of dihydroxybenzene

- isomers, *J. Electroanal. Chem.* 890 (2021), <https://doi.org/10.1016/j.jelechem.2021.115232>.
- [27] T.T. Liu, M. Zhou, Y.X. Pu, L.Q. Liu, F.F. Li, M.S. Li, M.X. Zhang, Silver nanoparticle-functionalized 3D flower-like copper (II)-porphyrin framework nanocomposites as signal enhancers for fabricating a sensitive glutathione electrochemical sensor, *Sens. Actuators B Chem.* 342 (2021), <https://doi.org/10.1016/j.snb.2021.130047>.
- [28] H. Chen, T. Yang, F. Liu, W. Li, Electrodeposition of gold nanoparticles on Cu-based metal-organic framework for the electrochemical detection of nitrite, *Sens. Actuators B Chem.* 286 (2019) 401–407, <https://doi.org/10.1016/j.snb.2018.10.036>.
- [29] C. Wang, F.J. Cao, Y.D. Ruan, X.D. Jia, W.Y. Zhen, X.E. Jiang, Specific generation of singlet oxygen through the russell mechanism in hypoxic tumors and GSH depletion by Cu-TCPP Nanosheets for cancer therapy, *Angew. Chem. Int. Ed.* 58 (2019) 9846–9850, <https://doi.org/10.1002/anie.201903981>.
- [30] A.U. Alam, M.J. Deen, Bisphenol A electrochemical sensor using graphene oxide and β -cyclodextrin-functionalized multi-walled carbon nanotubes, *Anal. Chem.* 92 (2020) 5532–5539, <https://doi.org/10.1021/acs.analchem.0c00402>.
- [31] C.F. Coutinho, M.O. Silva, M.L. Calegaro, S.A. Machado, L.H. Mazo, Investigation of copper dissolution in the presence of glyphosate using hydrodynamic voltammetry and chronoamperometry, *Solid State Ion.* 178 (2007) 161–164, <https://doi.org/10.1016/j.ssi.2006.10.027>.
- [32] M. Aguirre, S.E. Urreta, C.G. Gomez, A Cu^{2+} -Cu/glassy carbon system for glyphosate determination, *Sens. Actuators B Chem.* 284 (2019) 675–683, <https://doi.org/10.1016/j.snb.2018.12.124>.
- [33] A. Khenifi, Z. Derriche, C. Forano, V. Prevot, C. Mousty, E. Scavetta, B. Ballarin, L. Guadagnini, D. Tonelli, Glyphosate and glufosinate detection at electrogenerated NiAl-LDH thin films, *Anal. Chim. Acta* 654 (2009) 97–102, <https://doi.org/10.1016/j.aca.2009.09.023>.
- [34] J.S. Noori, M. Dimaki, J. Mortensen, W.E. Svendsen, Detection of glyphosate in drinking water: a fast and direct detection method without sample pretreatment, *Sensors* 18 (2018), <https://doi.org/10.3390/s18092961>.
- [35] F.C. Moraes, L.H. Mascaro, S.A. Machado, C.M. Brett, Direct electrochemical determination of glyphosate at copper phthalocyanine/multiwalled carbon nanotube film electrodes, *Electroanalysis* 22 (2010) 1586–1591, <https://doi.org/10.1002/elan.200900614>.
- [36] J.S. Santos, M.S. Pontes, E.F. Santiago, A.R. Fiorucci, G.J. Arruda, An efficient and simple method using a graphite oxide electrochemical sensor for the determination of glyphosate in environmental samples, *Sci. Total Environ.* 749 (2020), <https://doi.org/10.1016/j.scitotenv.2020.142385>.

Rui Jiang is studying for her master degree in School of Food Science and Technology, Jiangnan University, P. R. China. Her current research interests are the fabrication of nanomaterials and the manufacture of novel composite electrode materials.

Yue-Hong Pang is currently an associate professor in Jiangnan University, P. R. China. Her current research interests are the studies of novel properties of materials such as functionalized nanomaterials and their application for electrochemical sensors.

Qiu-Yu Yang is studying for her master degree in School of Food Science and Technology, Jiangnan University, P. R. China. Her current research interests focus on synthesis of novel nanomaterials and its application in electrochemistry.

Chao-Qun Wan is studying for her master degree in School of Food Science and Technology, Jiangnan University, P. R. China. Her current research interests focus on synthesis of functionalized nanomaterials and its application in electrochemistry.

Xiao-Fang Shen* is currently a professor in Jiangnan University, P. R. China. His research interests include the fabrication of novel nanomaterials and their application for electrochemical sensors.